REGIONAL LUNG STRAINS VIA A VOLUMETRIC MASS CONSERVING OPTICAL FLOW MODEL

Mohammadreza Negahdar[a] and Amir A Amini[a]
[a] Medical Imaging Laboratory, Department of Electrical and Computer Engineering,
University of Louisville, Louisville, KY

ABSTRACT

The main function of the respiratory system is gas exchange. Since many disease or injury conditions can cause biomechanical or material property changes that can alter lung function, there is great interest in measuring regional lung function and regional mechanical changes. The mechanical properties of lung parenchymal tissue are both elastic and dissipative, as well as being highly nonlinear. A novel lung-specific optical flow energy function for computing motion field from planar CT images was previously proposed. The main advantage of the proposed optical flow framework is the possibility to enforce physical constraints on the numerical solutions. In this paper, a 3-D extension of the aforementioned technique is proposed and the principal tissue strains from the 3-D displacement field are derived. Both the 3-D calculated deformation fields and strains are evaluated on a contracting/expanding simulated sponge volume simulating lung motion and POPI-model data from a human subject.

Index Terms: Deformable Image Registration, X-ray Computed Tomography, Optical Flow, Lung Motion, Lung Mechanics .

1. INTRDUCTION

The mechanical properties of lung tissue has been subject of scientific investigations ever since it was first realized that lung elastic recoil plays a crucial role in breathing [1]. Furthermore, a variety of important diseases involve significant alterations in lung tissue mechanics [2, 3]. For example, elastic recoil is markedly elevated in pulmonary fibrosis [4] and surfactant deficiency [5] and can be greatly reduced in emphysema [6]. In fact, virtually all pulmonary diseases of either the obstructive or restrictive classification involve some abnormality of lung tissue mechanics [2]. While the mechanical changes associated with the change of the material properties originate at a regional level, they are largely asymptomatic and invisible to global measures of lung function until they have advanced significantly and have aggregated. Therefore it would be desirable to have objective methods with which to evaluate and follow the progression of disease based on measurement of regional mechanics.

Imaging has long been used to study lung mechanics. Some investigators have studied the linkage between estimates of regional lung expansion and local lung ventilation as a measure of pulmonary function [7, 8]. Two classes of metrics have been used in ventilation imaging: Hounsfield unit (HU) change and Jacobian of the deformation field. Both metrics are based on the assumption that regional ventilation is proportional to the regional volume/density change. However, clear discrepancies have been reported by several researchers [9-11].

Strain is a dimensionless quantity representing the percent change in length of a continuously deformable body. Although strain quantification has been the topic of significant interest in cardiac imaging, it has received little attention in the area of lung imaging. In this work, we present a novel approach to quantification of motion and mechanical strain in the lung from 4-D CT using a multi-scale optical flow deformable image registration method.

2. METHODS

2.1 Optical flow motion estimation

The basic assumption in standard optical flow estimation is grey value constancy assumption which is not particularly applicable to lung motion estimation because of changes of voxel intensity of lung with inflation. In the past a number of papers have evaluated and have proposed techniques for non-rigid lung motion estimation [12-15]. These have for the most part been based on the free-form deformation paradigm. We include gradient constancy, mass conservation, as well as spatio-temporal smoothness in our optical flow framework [16] to more accurately model and estimate the deformation of the lung. The proposed optical flow framework has the advantage that it provides the possibility to enforce physical constraints on the flow field.

In order to derive a variational formulation for our proposed optical flow method, below, we list the constraints of interest. For additional details on the 2-D version of the algorithm, the reader is referred to [16].

(I) Ideally, the gray value of a voxel should not change after displacement:

$$I(X+W) = I(X) \tag{1}$$

In (1) I is the image intensity as a function of space and time, $X := (x, y, z, t)^T$, and $W := (u, v, w, 1)^T$ is the displacement vector field between two subsequent images. This assumption is also common to algorithms that use the sum of squares difference similarity metric. This is a nonlinear equation in u, v, and w. Its linearized version yields the well-known optical flow constraint [17]:

$$I_x u + I_y v + I_z w + I_t = 0 \tag{2}$$

(II) In anatomical CT images, we assume the imaged intensities follow a conservation principle in analogy to mass conservation in fluid flow. In fact, one can show that if it can be assumed that the Hounsfield unit is proportional to density then the two conservation principles are equivalent. Application of the conservation principle to a temporally varying image yields:

$$\nabla.(IV) + I_t = 0 \;\Rightarrow\; \nabla I.(V) + I(\nabla.V) + I_t = 0 \tag{3}$$

$$I_x u + I_y v + I_z w + I u_x + I v_y + I w_z + I_t = 0 \tag{4}$$

where $V = (u, v, w)$ is the velocity field. Equation (4) is a more general constraint for deformable object motion in comparison to the classic Horn-Schunck optical flow constraint equation shown in (2).

(III) In order to allow variations in the grey value and to help determine the displacement vector by a criterion that favors matching moving edges, a constraint based on image gradients is also incorporated:

$$\nabla I(X + W) = \nabla I(X) \tag{5}$$

(IV) Finally, in order to regularize the solution, spatio-temporal smoothness of the flow field is adopted:

$$|\nabla_4 \mathrm{u}|^2 + |\nabla_4 \mathrm{v}|^2 + |\nabla_4 \mathrm{w}|^2 \tag{6}$$

where $\nabla_4 := (\partial_x, \partial_y, \partial_z, \partial_t)^T$. Therefore, the energy functional that penalizes deviations from these model assumptions is measured by:

$$E(u, v, w) = E_D + \alpha E_S = \psi[|I(X + W) - I(X) + \beta(I\nabla.V)|^2 + \gamma|\nabla I(X + W) - \nabla I(X)|^2] + \alpha(\psi[|\nabla_4 \mathrm{u}|^2 + |\nabla_4 \mathrm{v}|^2 + |\nabla_4 \mathrm{w}|^2]) \tag{7}$$

The function $\psi(s^2) = \sqrt{s^2 + \varepsilon^2}$ is a modified L_1 norm which is convex and offers advantages in the minimization process namely robustness to outliers. Since ε is only utilized for numerical reasons, it can be set to a small fixed value (we chose 0.001).

Discretization yields a linear system of equations, which can be solved by successive over relaxation. Since the proposed method converges to the estimated motion in an iterative form, a multi-scale framework was used to speed up the calculation realizing significant computational savings. A multiresolution strategy helps deal with local minima as well.

2.2 Strain calculation

The deformation gradient tensor (DGT), $\boldsymbol{F}$, maps infinitesimal lengths between the undeformed and deformed state of a continuously deformable body:

$$\boldsymbol{F} = \begin{bmatrix} 1 + u_x & u_y & u_z \\ v_x & 1 + v_y & v_z \\ w_x & w_y & 1 + w_z \end{bmatrix} \tag{8}$$

Various kinematic descriptors of deformation can be calculated from the DGT. Because of the need for one-to-one correspondence between material points during continuous deformation, the determinant of the DGT, normally referred to as the Jacobian, has to be nonzero:

$$J = \det(\boldsymbol{F}) \tag{9}$$

In addition, in the absence of any deformation the Jacobian is equal to unity. Since, the deformation is assumed to be a continuous function of time, it is impossible for the Jacobian to be negative without passing through zero which was previously excluded from physical possibility. It therefore follows that for a continuous deformation to be physically possible, the Jacobian must be greater than zero. We took advantage of this fact to evaluate the accuracy of the calculated motion field. The degree of regional lung expansion is measured using the Jacobian of the displacement field which is directly related to specific volume change [18]. If the Jacobian is unity, there is no local expansion or contraction. If the Jacobian is greater than one, there is local tissue expansion; if the Jacobian is less than one, there is local tissue contraction.

DGT can be decomposed into stretch and rotation components:

$$\boldsymbol{F} = \boldsymbol{RU} \tag{10}$$

Where the $\boldsymbol{U}$ is the right stretch tensor and $\boldsymbol{R}$ is an orthogonal rotation tensor. The Cauchy-Green deformation tensor is defined as:

$$\boldsymbol{C} = \boldsymbol{F}^T\boldsymbol{F} = \boldsymbol{U}^2 \tag{11}$$

The concept of strain may be used to evaluate how much a given displacement differs locally from a rigid body displacement. The Lagrangian strain tensor, $\boldsymbol{E}$, is then given by:

$$\boldsymbol{E} = \frac{1}{2}(\boldsymbol{C} - \boldsymbol{I}) = \frac{1}{2}(\boldsymbol{F}^T\boldsymbol{F} - \boldsymbol{I}) \tag{12}$$

where **I** is the identity matrix. From the Lagrangian strain tensor we can calculate the various normal, shear, and principal strain values which describe the regional deformation of the lung.

Eigenvalue decomposition on the Lagrangian strain tensor yields the three principal strain values. The principal strain vectors are the corresponding eigenvectors and correspond to the directions of the principal axes of the reciprocal strain ellipsoid. The maximum, medium, and minimum eigenvalue are called the maximum, medium, and minimum principal strain, respectively. The maximum principal strain relates to maximum elongation and the minimum strain relates to maximum compression.

2.3 Assessment of image registration accuracy

For both qualitative and quantitative evaluation of the proposed method, a synthetic dataset and the POPI-model dataset [19] has been used. In the POPI-model dataset, 41 homologous landmarks were defined by experts in each of the 3-D volumes that make up this 4-D CT dataset with voxel dimensions 0.97 x 0.97 x 2 mm. We report here the accuracy of our optical flow method to the known expert-defined landmarks of the POPI-model.

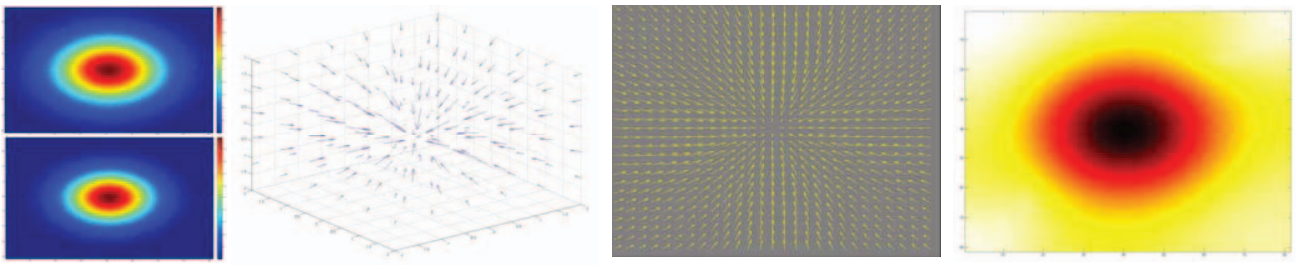
We applied the computed deformation to the ground truth point set in consecutive phases and compared estimated positions to the actual positions of the ground truth points. The differences between the estimated positions with the actual position are referred to as ground truth discrepancies. The registration result is reported as $\bar{\mu}_{gt} \pm \sigma_{\mu_{gt}}$ where $\bar{\mu}_{gt}$ denotes the average of all ground truth discrepancies and $\sigma_{\mu_{gt}}$ is the standard deviation.

Additionally, the Jacobian of the deformation field was evaluated to analyze physically plausibility of the computed deformation. In particular we expect that a deformation should be bijective. Regions where the deformation field is not bijective are commonly referred to as singularities. The determinant of the Jacobian of the deformation field was calculated at every point. This specified for each point whether local expansion or contraction had taken place. Any point where Jacobian is zero is a singularity in the deformation field. Additionally, a negative Jacobian implies a deformation that is physically not permissible.

3. RESULTS

Since the respiratory motion of the lung can be simplified and modeled as a time varying contraction and expansion [20], a volumetric sponge model which undergoes contraction and expansion has been used to evaluate the accuracy of the strain calculation method. Figure 1 displays the estimated motion and the calculated strain in glyph ellipsoid representation for a contracting sponge.

Figure 2 displays results from two volumetric images between phases P30 and P40 (volumetric frames 4 and 5) of the POPI-model. The average resulting error over the expert-defined homologous landmarks over all 10 phases was 1.12 ± 0.80 mm. Figures 2(b) and 2(c) display the calculated motion field between the same two phases. To compare the accuracy of our proposed technique with previously published work, Castillo et al.'s method



(a) (b) (c) (d)

Fig. 1: (a) Cross section of a contracting volumetric sponge $I(x,y,z,t) = \exp\left(-(x-\mu t)^2 - (y-\nu t)^2 - (z-\omega t)^2\right)$ for time points $t = 1$ and $t = 1.1$. (b) The three dimensional calculated motion field. (c) Axial cross section of the calculated motion field in (b) corresponding to the same axial location shown in (a). (d) Minimum principal component (contraction component) of the calculated strain tensor corresponding to the cross sections displayed in (a).

[12] which included a combined compressible local-global method achieved a mean registration error of 1.59 ± 1.43 mm on CT images with a voxel size of 0.97-1.16 x 0.97-1.16 x 2.5 mm while the compressible optical flow method by Wildes [21] achieved 1.68 ± 1.43 mm of error for the same dataset. Compared to these registration results we have been able to obtain smaller errors. The computational time to arrive at the motion field between two volumetric frames was on average 74 minutes on a Dell 5160 platform with a quad-core Xeon 3.00 GHz processor.

To further evaluate correctness of the deformable registration, singularity assessment was performed in order to ensure that registrations represented meaningful and physically plausible deformations. Figure 2(d) shows color-coded Jacobian of the POPI-model data between P30 and P40. As expected, there is no singularity in the calculated registration. In fact, the incorporated spatio-temporal regularization in the optical flow formulation (equation (6)) is the reason why singularities are averted. Figure 2(e) and 2(f) display the maximum and minimum 3-D principal strains illustrated for the mid-coronal slice of figure 2(a). In figure 2(g), the two strain images were combined using RGB channel combination with the R channel corresponding to the maximum component and B channel corresponding to minimum component. The G channel was set to zero.

The robustness of the proposed motion estimation and strain calculation method has been evaluated on the deforming sponge volume in the presence of Gaussian noise with different variances added to temporal volumetric images for both times $t = 1$ and $t = 1.1$. Figure 3 shows the relative root mean squared error (RRMS) between the true and estimated motion as well as the estimated maximum, medium, and minimum principal strain and corresponding ground-truth quantities. As may be seen, the errors for the motion field are significantly smaller than those for the strain. Clearly, spatio-temporal smoothness in the optical flow energy function has alleviated the effect of noise on the estimated motion while the derivative operator in calculation of DGT has amplified the effect of noise in the calculated strain tensor.

4. CONCLUSIONS

We have proposed a 3-D multiresolution optical flow framework based on the mass conservation principal and image gradient constancy. The proposed optical flow framework provides the possibility to enforce physical constraints on the velocity field to handle the difficulties inherent in the thoracic CT image registration problem.

Principal strains and directions were calculated starting from the deformation field produced by our optical flow framework. Strain calculations were validated with a volumetric sponge simulation exhibiting contraction.

REFERENCES

[1] E. R. Weibel, "What makes a good lung?," *Swiss medical weekly,* vol. 139, pp. 375-386, 2009.

[2] B. Suki, and J. H. T. Bates, "Lung tissue mechanics as an emergent phenomenon," *Journal of Applied Physiology,* vol. 110, pp. 1111-1118, 2011.

[3] J. H. T. Bates, G. S. Davis, A. Majumdar *et al.*, "Linking parenchymal disease progression to changes in lung mechanical function by percolation," *Am. J. Respir. Crit. Care Med.,* vol. 176, pp. 617-623, 2007.

[4] J. Yernault, M. d. Jonghe, A. d. Coster *et al.*, "Pulmonary mechanics in diffuse fibrosing alveolitis," *Bull Physiopathol Respir,* vol. 11, pp. 231-244, 1975.

[5] D. Massaro, L. Clerch, D. Temple *et al.*, "Surfactant deficiency in rats without a decreased amount of extracellular surfactant," *J Clin Invest,* vol. 71, pp. 1536-1543, 1983.

[6] I. Greaves, and H. Colebatch, "Elastic behavior and structure of normal and emphysematous lungs post mortem," *Am Rev Respir Dis,* vol. 121, pp. 127-136, 1980.

[7] T. A. Sundaram, and J. C. Gee, "Towards a model of lung biomechanics: pulmonary kinematics via registration of serial lung images.," *Medical Image Analysis,* vol. 9, pp. 524-537, 2005.

[8] M. H. Tawhai, and C. L. Lin, "Image-based modeling of lung structure and function," *J Magn Reson Imaging,* vol. 32, pp. 1421-1431, 2010.

[9] R. Castillo, E. Castillo, J. Martinez *et al.*, "Ventilation from four-dimensional computed tomography: density versus Jacobian methods," *Physics in Medicine and Biology,* vol. 55, pp. 4661-4685, 2010.

[10] K. Ding, K. Cao, R. E. Amelon *et al.*, "Comparison of Intensity- and Jacobian-based estimates of lung regional ventilation," *Medical Image Analysis for the Clinic: A Grand Challenge*, 2010, pp. 49-60.

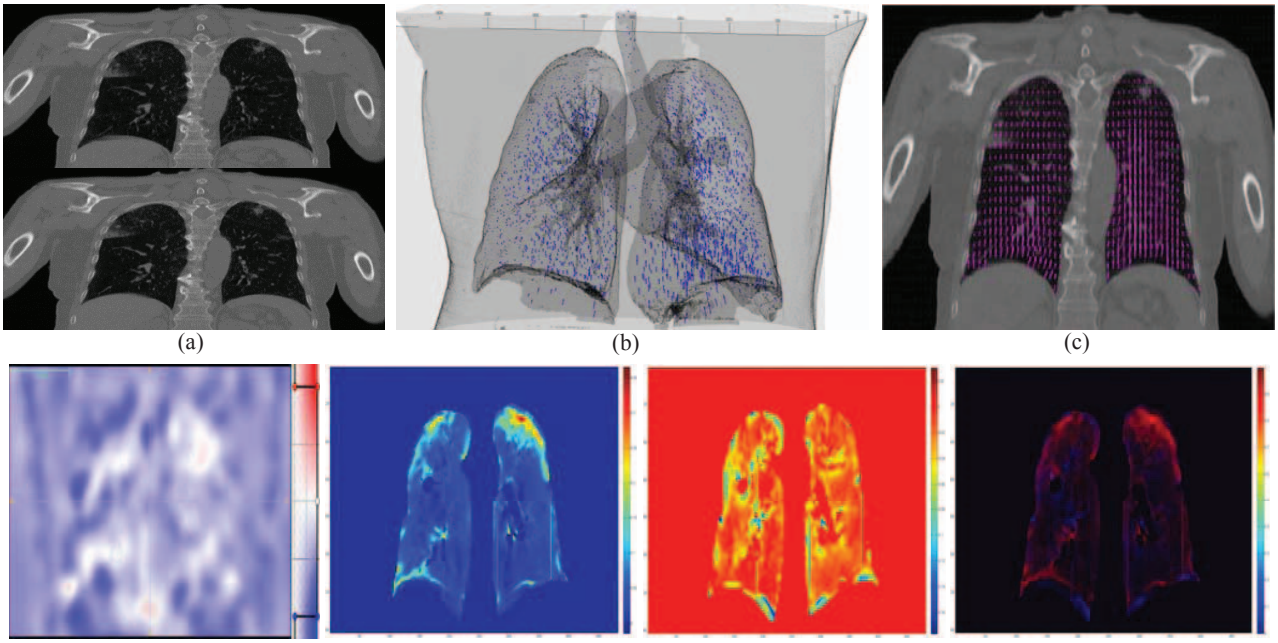


Fig. 2: (a) Coronal plane of the POPI-model in max-inhale (top) and max-exhale (bottom) respiration phase. (b) The calculated volumetric motion field. (c) The coronal plane of the calculated motion field. (d) A color coded Jacobian image with the scale going from 0.3 (blue) to 1.7 (red). (e) The maximum principal strain component. (f) The minimum principal strain component. (g) The superimposition of both maximum (red) and minimum (blue) principal strain components.

[11] T. Yamamoto, S. Kabus, T. Klinder *et al.*, "Four-dimensional computed tomography pulmonary ventilation images vary with deformable image registration algorithms and metrics," *Medical Physics,* vol. 38, pp. 1348-1358, 2011.

[12] E. Castillo, R. Castillo, Y. Zhang *et al.*, "Compressible image registration for thoracic computed tomography images," *Journal of Medical and Biological Engineering,* vol. 29, pp. 236-247, 2009.

[13] K. Cao, G. E. Christensen, K. Ding *et al.*, "Intensity-and-landmark-driven, inverse consistent, B-Spline registration and analysis for lung imagery," *Second International Workshop on Pulmonary Image Analysis*, 2009, pp. 137-148.

[14] Y. Yin, E. A. Hoffman, and C.-L. Lin, "Mass preserving non-rigid registration of CT lung images using cubic B-spline," *Medical Physics,* vol. 36, pp. 4213-4222, 2009.

[15] M. Staring, S. Klein, J. H. C. Reiber *et al.*, "Pulmonary image registration with elastix using a standard intensity-based algorithm," *Medical Image Analysis for the Clinic: A Grand Challenge*, 2010, pp. 73-79.

[16] M. Negahdar, and A. A. Amini, "Planar deformable motion estimation incorporating mass conservation and image gradient constancy," *IEEE International Symposium on Biomedical Imaging (ISBI): From Nano to Macro*, 2011, pp. 536-540.

[17] B. K. P. Horn, and B. G. Schunck, "Determining optical flow," *Artificial Intelligence,* vol. 17, pp. 185-203, 1981.

[18] J. M. Reinhardt, K. Ding, K. Cao *et al.*, "Registration-based estimates of local lung tissue expansion compared to xenon-CT measures of specific ventilation," *Medical Image Analysis,* vol. 12, pp. 752-763, 2008.

[19] J. Vandemeulebroucke, D. Sarrut, and P. Clarysse, [The POPI-model, a point-validated pixel-based breathing thorax model], Toronto, Canada(2007).

[20] M. Negahdar, and A. A. Amini, "Estimation of affine motion from projection data using a mass conservation model," *33rd Annual International Conference of the IEEE Engineering in Medicine and Biology Society, 2011. EMBS '11*, 2011, pp. 8041-8044.

[21] R. P. Wildes, M. J. Amabile, A.-M. Lanzillotto *et al.*, "Recovering estimates of fluid flow from image sequence data," *Computer Vision and Image Understanding,* vol. 80, pp. 246-266, 2000.

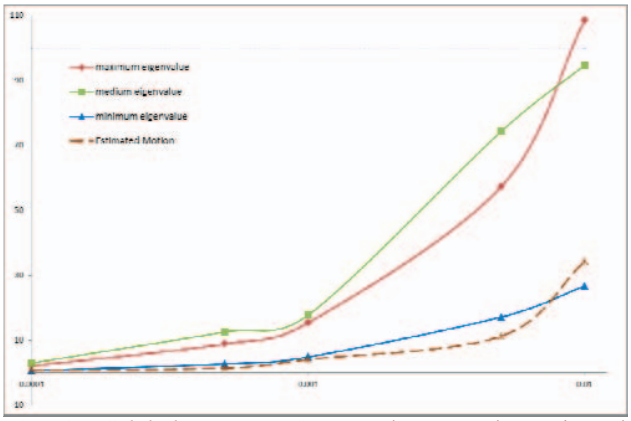


Fig. 3: *Solid lines:* RRMS error between the estimated Lagrangian principal strains (maximum, medium, and minimum) and corresponding ground-truth quantities for the entire image volume. *Dashed line:* RRMS error between the estimated motion and the true motion. Abscissa: variance of additive Gaussian noise. Ordinate: RRMS error in percent.